

Electronic Supplementary Material (ESI) for Lab on a Chip

Monitoring Few Molecular Binding Events in Scalable Confined Aqueous Compartments by Raster Image Correlation Spectroscopy (CADRICS)[†]

G. Arrabito^a, F. Cavaleri^a, V. Montalbano^a, V. Vetri^{a,b,*}, M. Leone^{a,b}, B. Pignataro^{a,b*}

a. Dipartimento di Fisica e Chimica, Università degli Studi di Palermo, Ed. 17, V.le delle Scienze 90128 Palermo, Italy.

b. Aten Center, Università degli Studi di Palermo, Ed. 18, V.le delle Scienze, 90128 Palermo, Italy.

* Corresponding authors: valeria.vetri@unipa.it, bruno.pignataro@unipa.it.

[†] G. Arrabito and F. Cavaleri equally contributed to this work.

Keywords: Confined Droplets, Microarrays, Inkjet Printing, Raster Image Correlation Spectroscopy, Intermolecular Interactions

Table of Contents:

-Water-in-oil droplet array fabrication

-RICS experimental results

-Two components fit in RICS

Water-in-oil droplet array fabrication

The experimental conditions for inkjet printing operation can be better visualized in Figure S1 in which the inverse of Ohnesorge number ($Z = 1/Oh$) is plotted against the Reynold number according to Derby¹. Ohnesorge (Oh) and Reynold (Re) numbers are given by:

$$Oh = \frac{\mu}{\sqrt{\rho\sigma L}} \quad Re = \frac{\rho v L}{\mu}$$

Where

ρ is the liquid density (g/cm³)

σ is the surface tension (dyne/cm)

L is the characteristic length scale (i.e drop diameter)

v is the velocity of the fluid (m/s)

μ is the dynamic viscosity of the fluid (cP)

Whereas Oh relates the viscous forces to surface tension forces, Re relates the inertial forces to the viscous forces.

The red dot in the Scheme 1 defines the experimental conditions of the liquid ink here used (100 mM potassium phosphate, 0.05 % tween 20). The low viscosity of the aqueous ink determines satellites which would render the printing process not reproducible. On the other hand, the grey dot corresponds to the experimental condition of the mineral oil, which has high viscosity and low density, respectively 30.0 cP and 0.82 g/cm³.

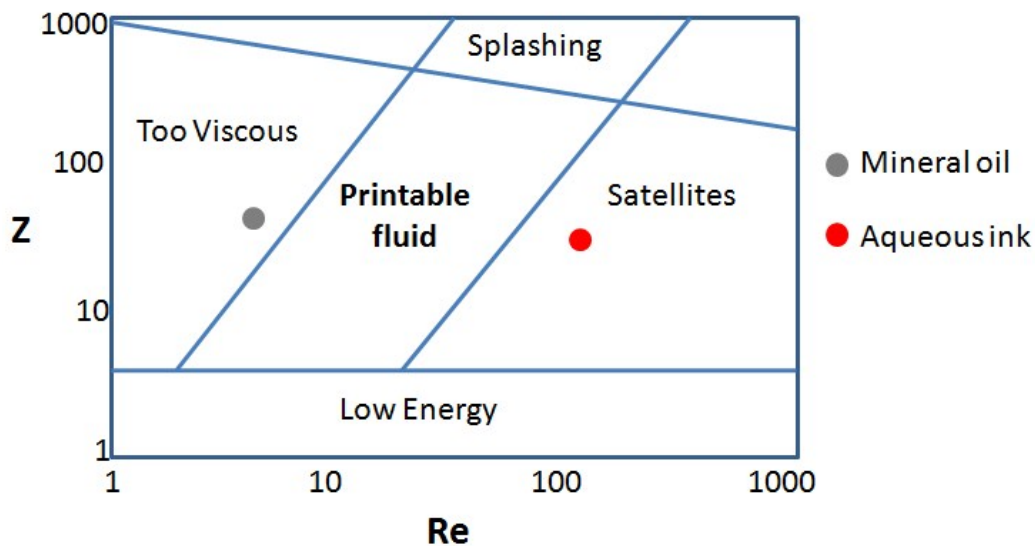


Fig. S1. Printing regimes in inkjet printing. The coordinate system defined by the Reynolds and Ohnesorge numbers illustrate the regime of fluid properties in which inkjet printing is possible. Red and grey dot represent experimental points for, respectively, aqueous ink and mineral oil.

Inkjet printing dispensing of mineral oil was easily accomplished by standard double pulse waveforms, increasing ink temperature at 33 °C in order to reduce dynamic viscosity (30 cps at 25 °C) obtaining droplets with long tails (> 200 μm) having velocities in the range 5 to 15 m/s (Fig. S1).

The assembly of mineral oil droplets arrays on glass surfaces is easily accomplished (Fig. S1-S3) by employing conventional piezoelectric waveforms (Fig. S2). In the initial stage piezo is in a neutral or relaxed position in which chamber is at its maximum volume. During the rise time (t_R) voltage is increased, causing a deflection in the piezo which pulls the fluid to the nozzle exit in order to form the droplet. The time at which the piezo is stable in a deflected state is called dwell time t_D . During fall time (t_F), the piezo voltage is decreased in order to pinch-off droplet at the nozzle exit. Remarkably, the relative relaxation of the piezo in during t_F permits to pull the liquid thread back in the nozzle.

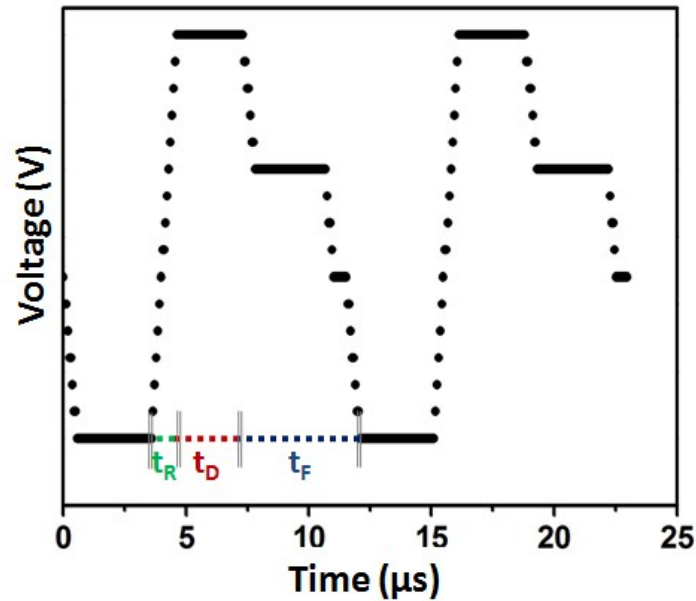


Fig. S2. Conventional double pulse waveform.

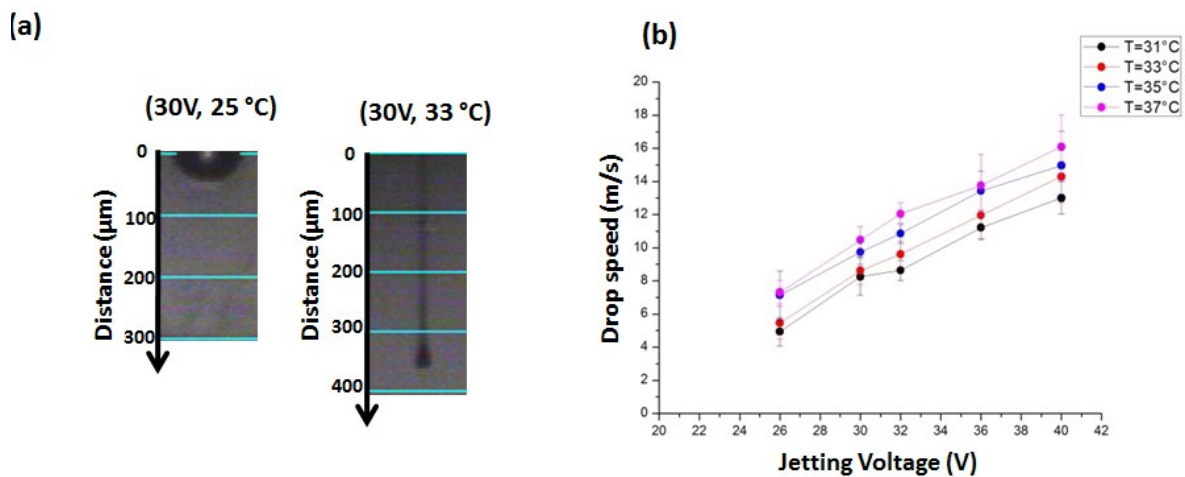


Fig. S3. Mineral oil droplet dispensing. (a). Stroboscopic images of 10 pL (nominal volume) mineral oil droplet pinching-off at nozzle at 25 °C (left) and at 33 °C (right). (b) Droplet speed (m/s) versus Jetting Voltage (V) for mineral oil droplet dispensing by double pulse waveforms at increasing temperature (31 °C – 37 °C).

Aqueous ink dispensing required a more careful investigation. In order to allow the printing process of such low viscosity ink, we optimized the waveform signal in order to avoid satellites formation. There are two possibilities to avoid this. The first case occurs when the liquid thread ejected from the nozzle breaks up, and then the satellite and primary drop recombine to form a single drop². This condition is not considered in this work and, thus, it

will be omitted in the discussion. The second case is constituted by the contraction of the liquid thread ejected from nozzle in single droplet without phenomena of multiple breakups. We preferred to choose this method to better control droplet generation allowing for more reproducible results. In this case, the liquid thread ejected from the nozzle is able to contract into a single drop without breaking up if the length of liquid thread at pinch-off, l_b , does not exceed a limiting value l_b^* as from the following equation^{2,3}:

$$\frac{l_b}{R_{noz}} < \zeta \frac{1}{\alpha_{max}^*} + 2 = \frac{l_b^*}{R_{noz}}$$

Where

R_{noz} is the radius of the nozzle;

$\zeta = (C_2 - C_1) \cdot a$ is a measure of the times difference for the formation of the droplets at the nozzle exit C_1 and at complete pinch-off C_2 , being a constant value. ζ is usually comprised between 0.9 and 1.1;

α_{max}^* is given by the following expression:

$$\alpha_{max}^* = \sqrt{\frac{1}{2}x^2(1-x^2) + \frac{9}{4}x^4} - \frac{3}{2}Oh \cdot x^2$$

where

$$x^2 = \frac{1}{2 + \sqrt{18} \cdot Oh}$$

From this model, it turns out that for our aqueous ink, by considering that tween-20 decreases surface tension up to 35 mN/m, we obtain that Oh is almost 0.036 and α_{max}^* is

equal to 0.756 which determine a $\frac{l_b^*}{R_{noz}}$ ratio of about 3.5. This means that in order to avoid satellite formation, it is necessary to have a liquid length while pinching off at nozzle of not more than 60 μm , since radius of the nozzle is about 21 μm .

Double pulse waveform used for mineral oil dispensing produced long liquid thread ($> 60 \mu\text{m}$), so determining, as expected, a high number of satellites droplets (see **Figure S4**).

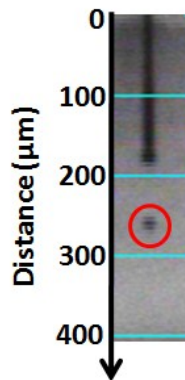


Fig. S4. Stroboscopic image of 10 pL (nominal volume) Alexa 647 droplet (40 nM, 0.05% Tween-20) pinching-off at nozzle during emission (16 V) by double pulse waveform. Satellite droplet is marked in the red circle.

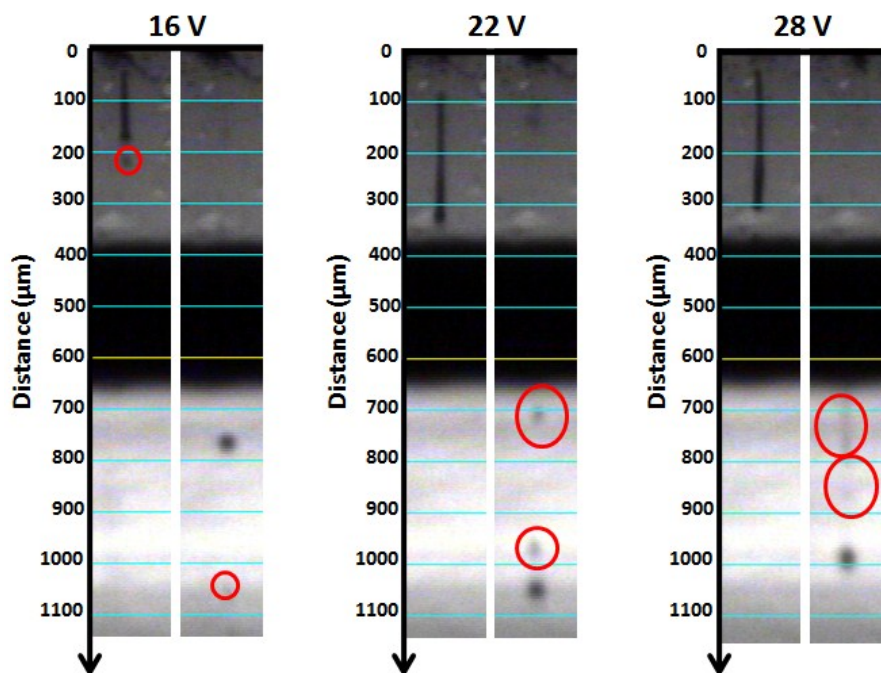


Fig. S5. Stroboscopic images of Atto-655 biotin (BTN*) (40 nM, 0.05 % tween 20) droplet dispensing by double pulse waveforms at various voltages (16 V – 22 V – 28 V). At each voltage, stroboscopic picture is taken while droplet is pinched-off (left figure) and when it reached 1000 μm to better show multiple breakups. Satellites droplets are encircled.

In order to avoid satellites formation during aqueous ink dispensing, we needed to tune waveform signal for reducing liquid length while pinching off at nozzle at values minor than

60 μm . To achieve that, we adapted a single pulse waveform signal (Fig. S5) instead of the conventional double pulse waveform (Fig. S3) in such a way to:

1. Increase the rise time (t_R) (which passed from 1 μs of double pulse waveform to 2.93 μs of single pulse waveform) in order to favour droplet formation at the nozzle.
2. Increase the fall time (t_F), i.e. the time at which the piezo voltage is decreased in order to pinch-off droplet at the nozzle exit. As to do so, we showed the possibility to decrease the onset of multiple breakup phenomena in the liquid thread minimizing the occurrence of satellite droplets⁴. We fixed fall time (t_F) to 16.9 μs – to be compared with 4.92 μs of double pulse waveform.

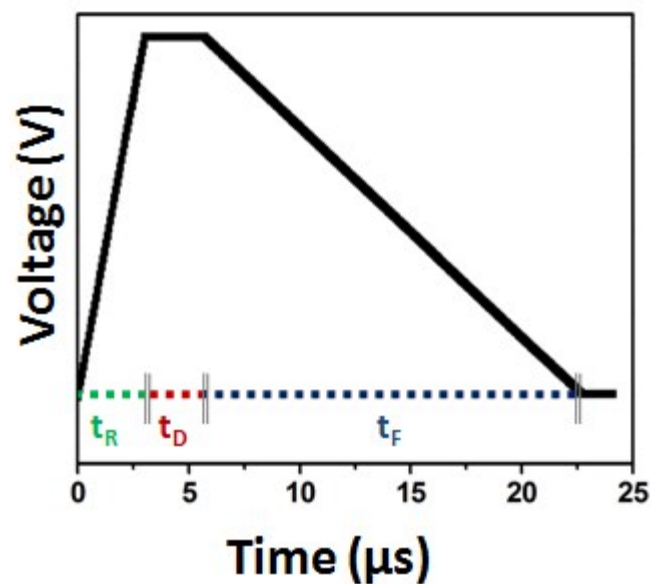


Fig.S6. Single pulse waveform specifically suited for aqueous inkjet printing.

We then investigated the liquid thread length while pinching-off at nozzle as a function of jetting voltages by using single pulse waveform signal pulse (**Fig. S6**). As clearly shown by stroboscopic figures (**Fig. S7.A**), low-to-intermediate jetting voltages (16 V - 22 V) allow for short liquid threads (minor than threshold of 60 μm) that rapidly coalesce into spherical droplets, whereas high voltages (28 V) determine liquid threads longer than threshold which

are prone to breakups and satellite formation. For this reason, we identified low voltages as the optimal condition for aqueous ink dispensing at velocities (around 6 m/s – see **Fig. S7.B**) sufficient for encapsulation into mineral oil droplets. Remarkably, droplet velocities are quite well distributed among different nozzles of the same print head (**Fig. S7.C**).

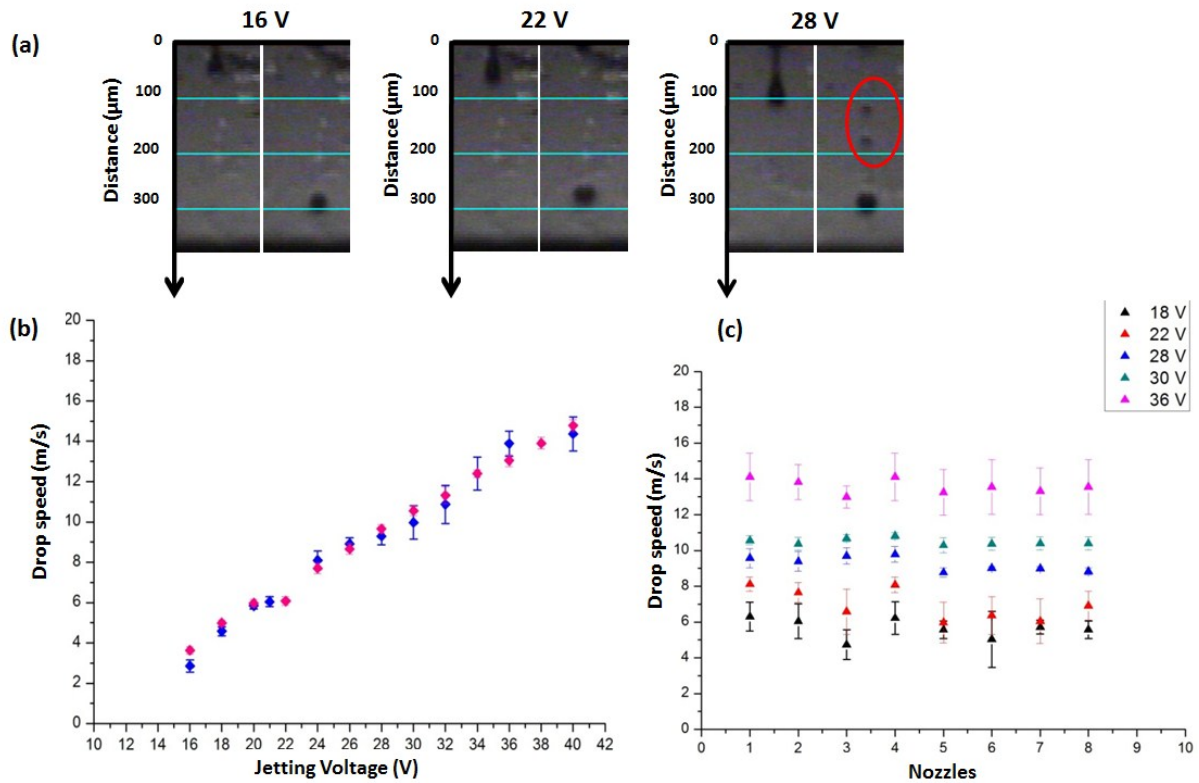


Fig. S7. Atto-655 biotin droplet dispensing by single pulse waveforms. **(a)** Stroboscopic images of 10 pL (nominal volume) BTN* (40 nM, 0.05 % tween 20) droplet pinching-off at nozzle at 16 V, 22 V and 28 V (left picture for each voltage), or when it reached almost 300 μm in the trajectory from nozzle. Satellites droplets are encircled. **(b)** Droplet speed (m/s) versus Jetting Voltage (V) for BTN* (40 nM) droplet in absence of STV (blu dots) or in presence of Streptavidin 10 nM (red dots). **(c)** Droplet velocity as a function of jetting nozzle for BTN* (40 nM) solution dispensing.

RICS experimental results

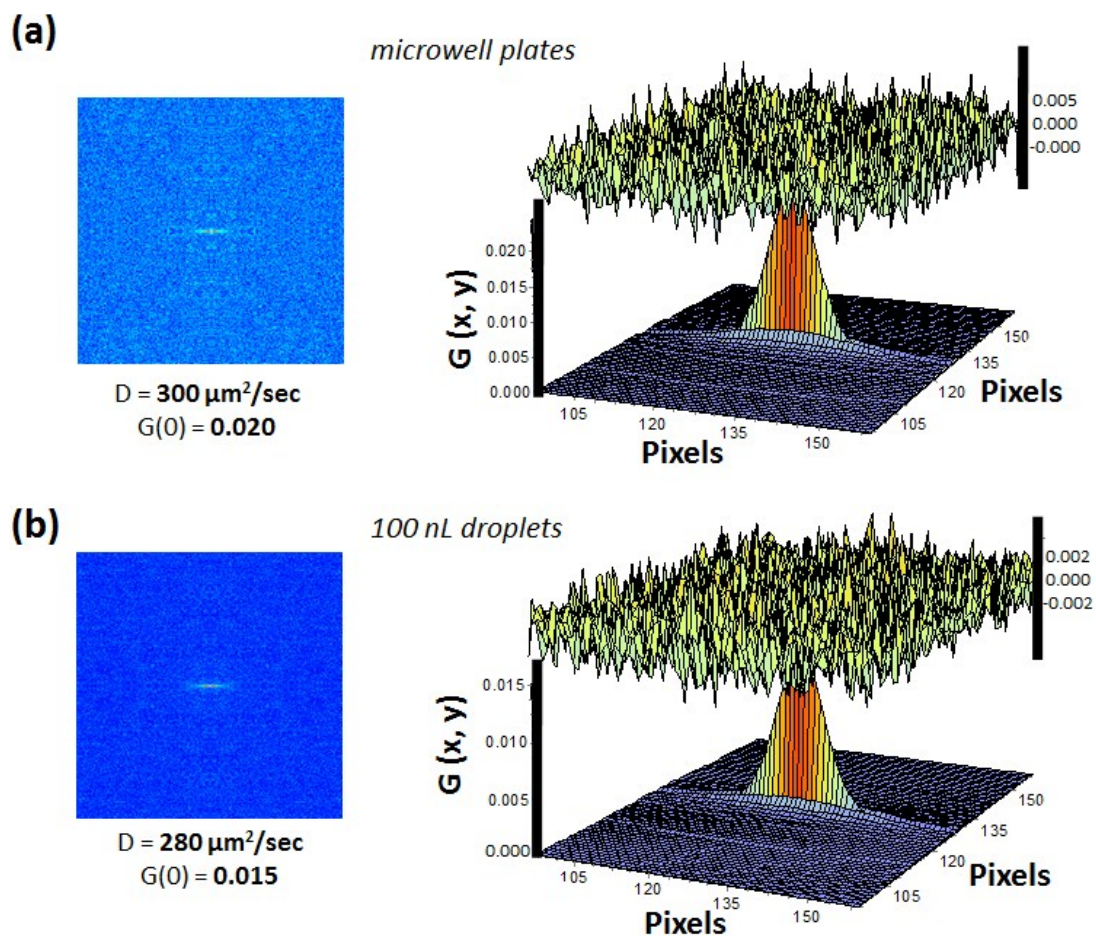


Fig. S8. RICS on Alexa 647 solution on 500 μL volume in microwell plates and on 100 nL droplets manually deposited. Spatial autocorrelation functions and relative fits with residuals of Alexa 647 (20 nM) in microwell plates (a) and on 100 nL droplets (b).

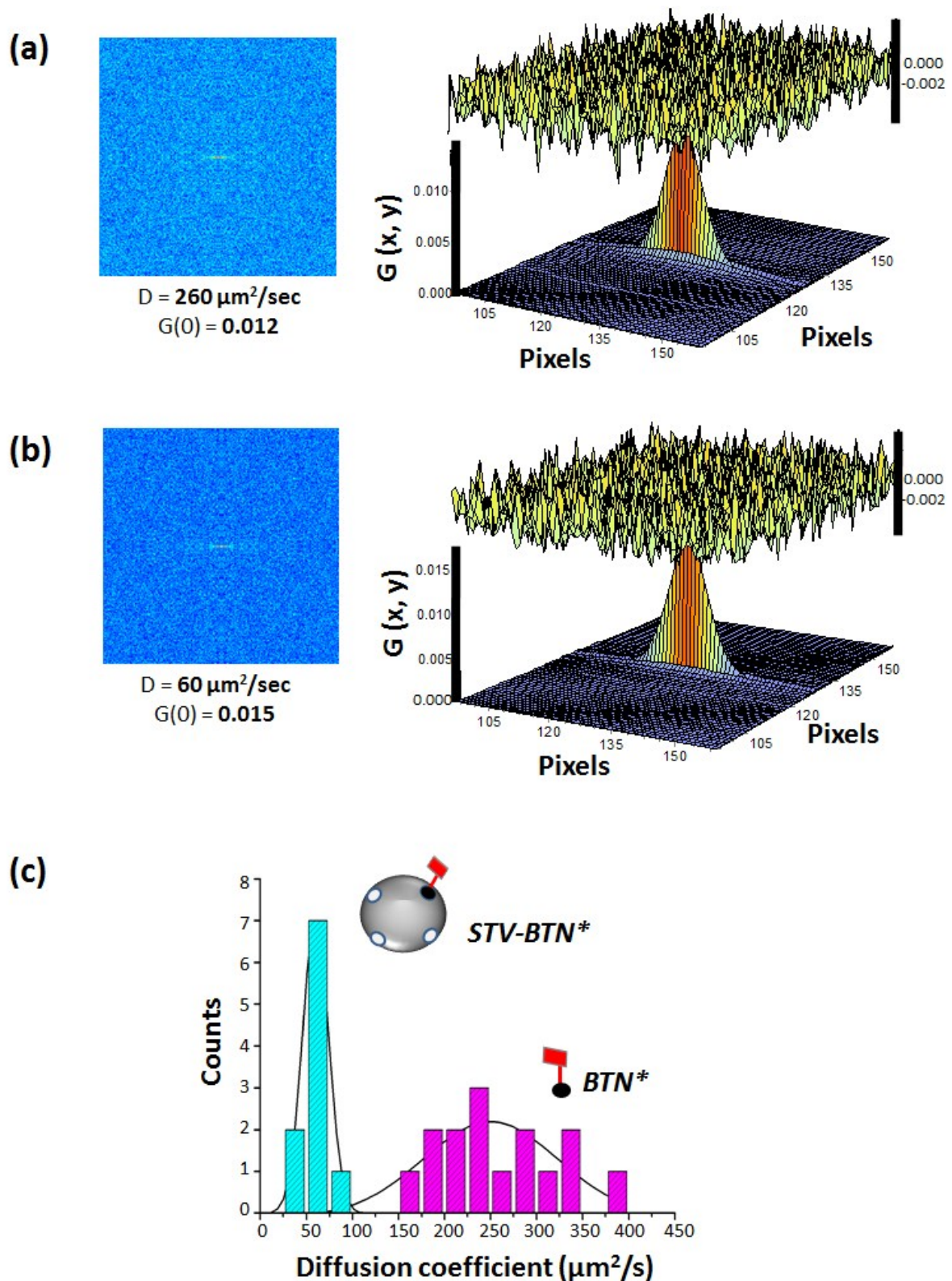


Fig. S9. Atto-655 biotin binding to STV obtained from measurements on 500 μL volume samples in microwell plates. Typical spatial autocorrelation functions and relative fits with residuals of of Atto655-biotin (BTN*) (20 nM) (a) and of the Streptavidin-Atto655-biotin (STV-BTN*) complex (b) obtained from microwell plates. In (c), histograms showing diffusion coefficient distribution for BTN* (light blue bars) and STV-BTN* complex (pink bars)

obtained from measurements in microwell plates. Black lines representing Gaussian distributions centered at D mean values are reported as an eye guidelines.

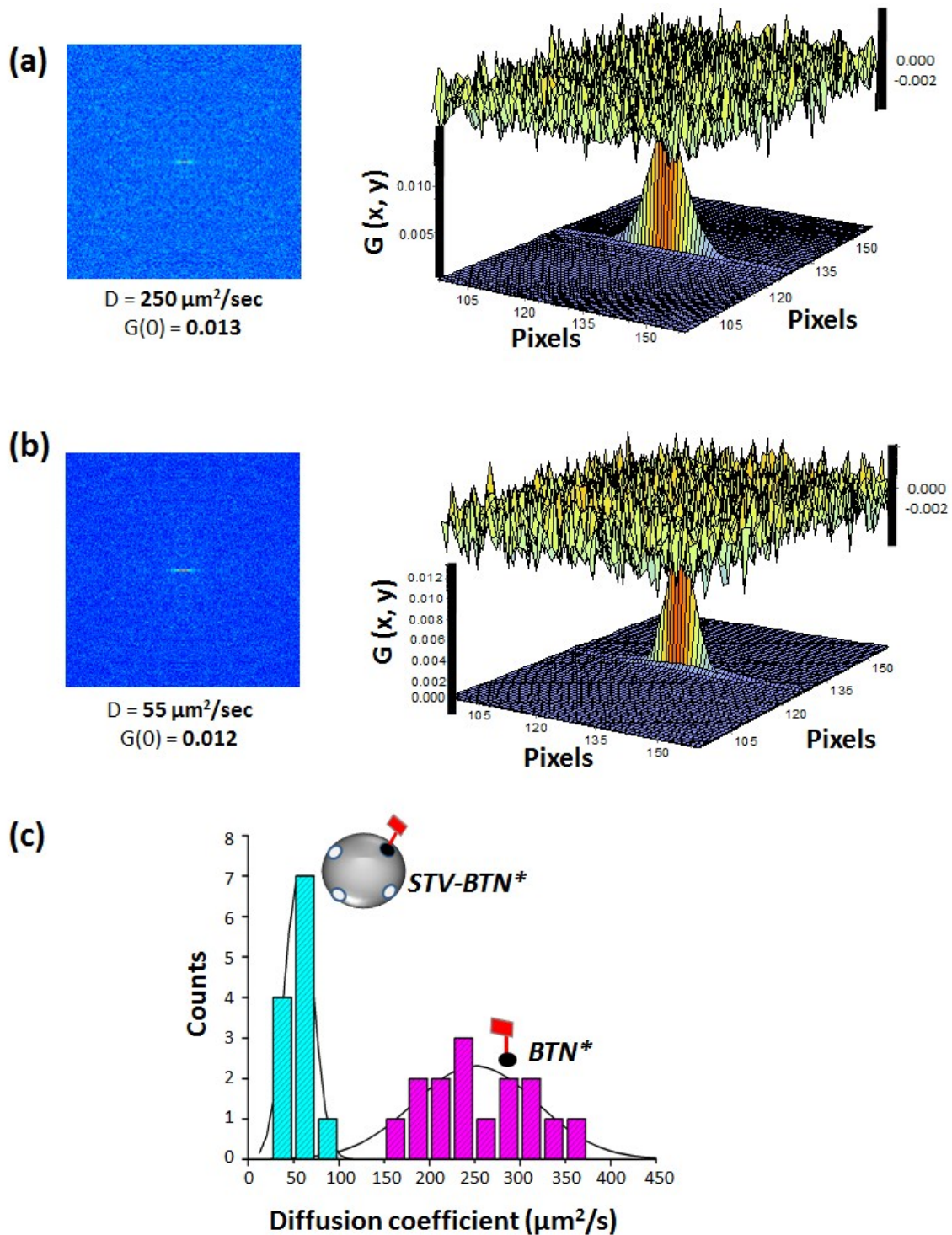


Fig. S10. Atto-655 biotin binding to STV in 100 nL droplets. Spatial autocorrelation functions and relative fits with residuals of BTN^* (20 nM) (a) and of the STV-BTN^* complex (b) obtained from 100 nL aqueous droplets. In (c), histograms showing diffusion coefficients distribution for BTN^* (light blue bars) and STV-BTN^* complex (pink bars) obtained from

measurements in 100 nL aqueous droplets. Black lines representing Gaussian distributions centered at D mean values are reported as an eye guidelines.

Volume (nL)	Diameter (μm)	Area (μm^2)	Roundness
10^0	220 ± 30	38000 ± 8500	0.88 ± 0.01
10^{-1}	90 ± 10	6200 ± 400	0.82 ± 0.02

Table S1. Comparison of droplet diameters, areas and roundness inkjet printed at different volumes (10^0 - 10^{-1} nL) in 10 nL mineral oil droplets. Values are averaged from 10 different aqueous droplets.

Volume (nL)	D (BTN*) ($\mu\text{m}^2/\text{s}$)	G(0)	D (STV-BTN*) ($\mu\text{m}^2/\text{s}$)	G(0)
$5 \cdot 10^4$	260.7 ± 60.6	0.015 ± 0.003	57.9 ± 8.9	0.012 ± 0.002
10^2	252.4 ± 50.1	0.012 ± 0.002	54.8 ± 9.1	0.013 ± 0.002
10^0	254.4 ± 51.1	0.018 ± 0.002	60.7 ± 10.5	0.015 ± 0.003
10^{-1} (*)	220.4 ± 51.8	0.014 ± 0.003	45.2 ± 14.6	0.015 ± 0.003

Table S2. Comparison of average diffusion coefficients (D) and G_0 values obtained from ten measurements on samples of different volumes ($5 \cdot 10^4$ – 10^0 nL). (*) Average of five measurements.

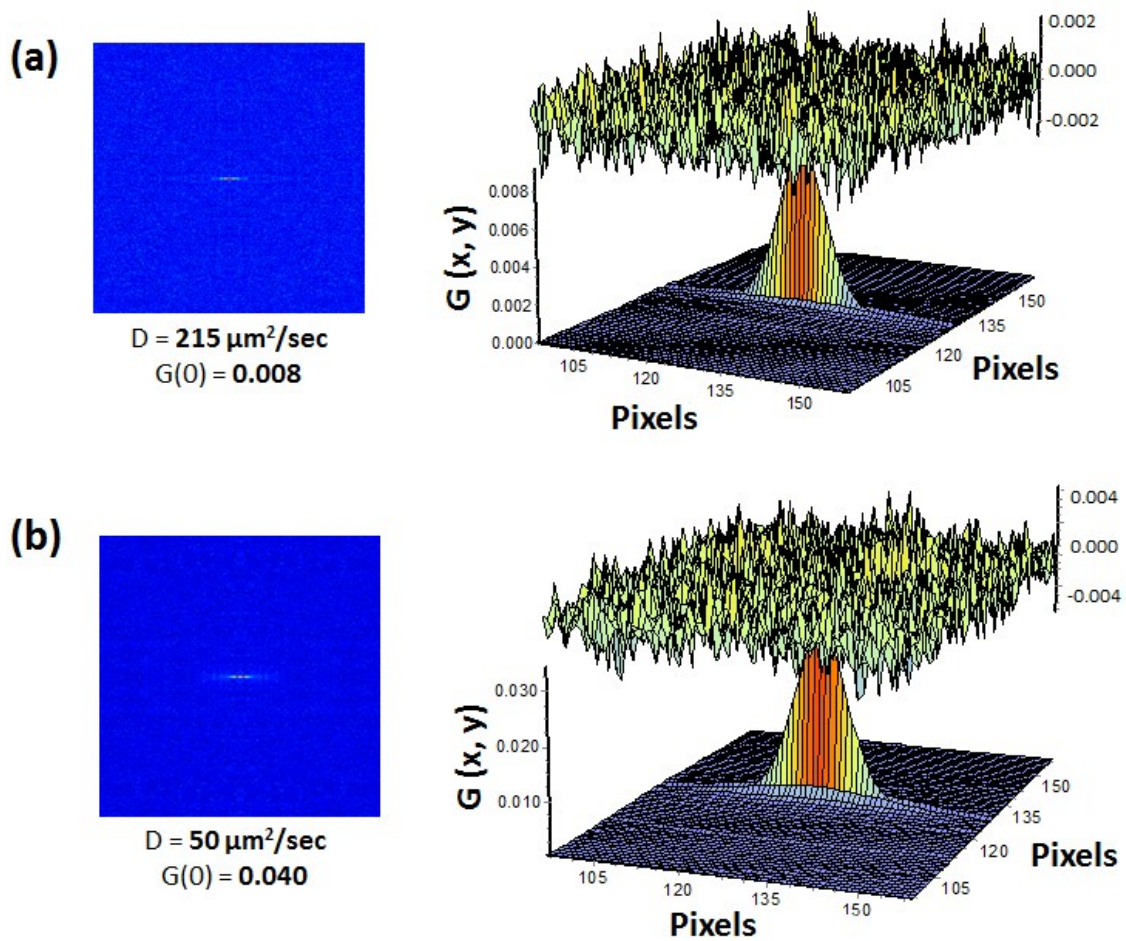


Fig. S11. Spatial autocorrelation functions and relative fits with residuals of of BTN* (40 nM) **(a)** and of the STV-BTN* complex in presence of the stoichiometric amount of STV (10 nM) **(b)** obtained from measurements on 100 nL droplets.

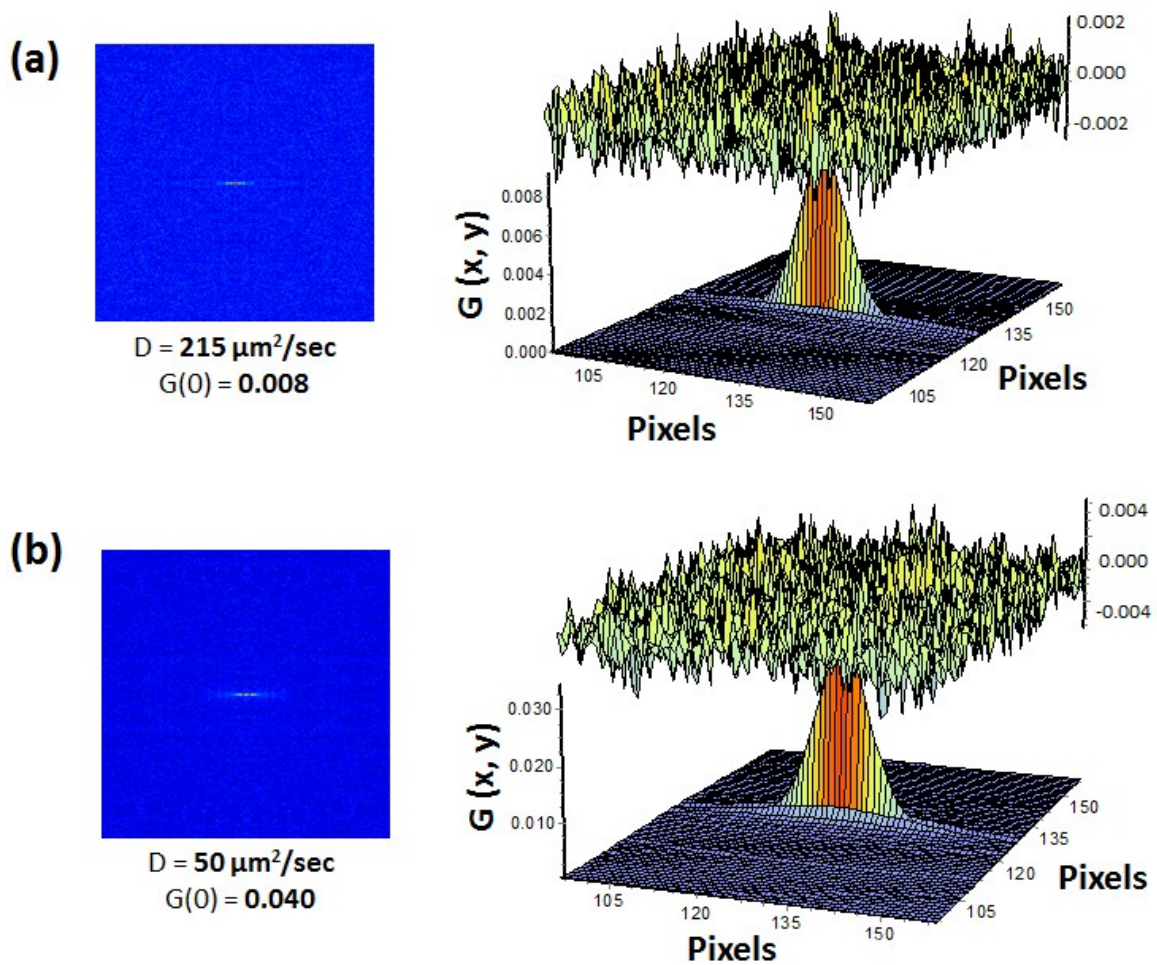


Fig. S12. Spatial autocorrelation functions and relative fits with residuals of BTN* (20 nM) **(a)** and of the STV-BTN* complex in presence of the stoichiometric amount of STV (10 nM) **(b)** obtained from measurements 1 nL droplets.

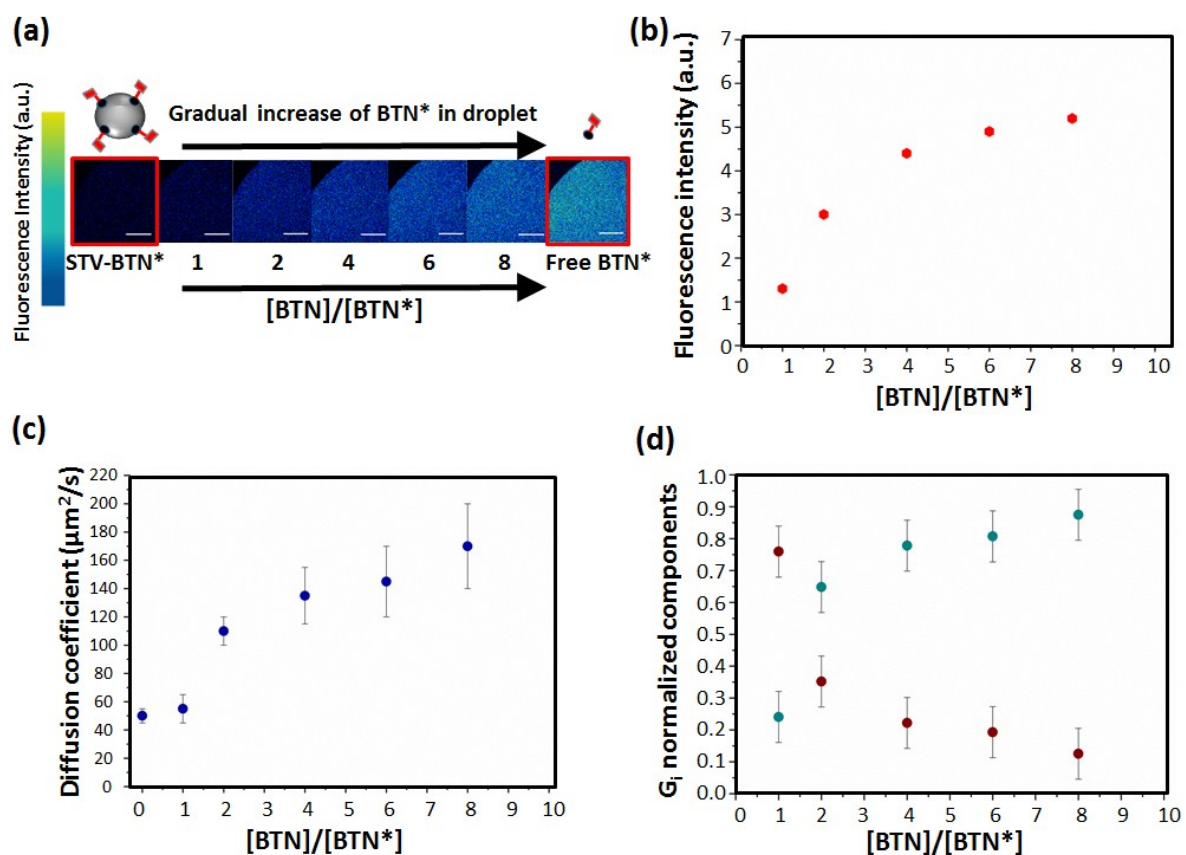


Fig. S13. Competitive inhibition reactions in 100 nL droplets. **(a)** 256x256 representative fluorescence confocal images of 100 nL drops injected in oil matrices. All aqueous droplets contain 40 nM BTN* -10 nM STV. [BTN]/[BTN*] ratio is progressively increased in the droplet - corresponding to [BTN] values of 40 nM, 80 nM, 160 nM, 240 nM and 320 nM. Drop on the right contains free BTN* as reference. Scale bar is equal to 100 μm. **(b)** Average fluorescence intensity measured in the droplets. **(c)** Diffusion coefficients obtained from one component RICS analysis as a function of molar fraction between BTN and BTN*. **(d)** Normalised amplitude $G_1(0)/G(0)$ (red dots) and $G_2(0)/G(0)$ (blue dots).

Two components fit in RICS

From FCS analysis, it is typically possible to extract the amplitude of the autocorrelation function value $G(0)$ which is inversely proportional to the total concentration of molecules in the analysed sample. In case of the analysis of multiple species, the value $G(0)$ can be expressed as the sum of two different G values, $G_1(0)$ related to the “slow” Atto 655-biotin species which are STV-BTN (BTN₃*), STV- BTN₂(BTN₂*), STV- BTN₃(BTN *) and STV-(BTN₄*),

and $G_2(0)$ ascribed to the “fast” unbound Atto655-biotin (BTN*) species. This is accordance with the equation expressing the autocorrelation function in multicomponents models⁵:

$$G(t) = \frac{\bar{n}_1^2}{(\bar{n}_1 + \bar{n}_2)^2} G_1(t) + \frac{\bar{n}_2^2}{(\bar{n}_1 + \bar{n}_2)^2} G_2(t)$$

in which $\bar{n}_1 = Q_1 \bar{N}_1$ being \bar{N}_1 the concentration of molecules of type 1 (for example the unbound species) and Q_1 is a measure of the molecular brightness.

From RICS it is also possible to carry out multicomponent analysis as described by Ilaste et al.⁶ who derived an analytical expression for autocorrelation function in case of two diffusing species with different diffusion coefficients. From their expression, it is possible to obtain:

$$G(0) = \frac{\gamma}{(\bar{n}_1 + \bar{n}_2)^2} \cdot (\bar{n}_1 + \bar{n}_2)$$

In which \bar{n}_1 and \bar{n}_2 are the concentrations of the species having molecular diffusion D_1 and

D_2 . By defining $G(0) = \frac{\gamma}{\bar{n}_1 + \bar{n}_2}$ and the molar fraction $\chi_i = \frac{\bar{n}_i}{\bar{n}_1 + \bar{n}_2}$, it is possible to obtain:

$$G(0) = G(0) \frac{\bar{n}_1}{\bar{n}_1 + \bar{n}_2} + G(0) \frac{\bar{n}_2}{\bar{n}_1 + \bar{n}_2}$$

Which finally gives:

$$G(0) = G(0) \cdot \chi_1 + G(0) \cdot \chi_2$$

This can be rewritten as:

$$G(0) = G(0)_1 + G(0)_2$$

In which we define $G_1 = G(0) \cdot \chi_1$ as the $G(0)$ value for the slow diffusing species - i.e. Atto 655 biotin is bound to streptavidin and $G_2 = G(0) \cdot \chi_2$ as the $G(0)$ value for the rapid diffusing species- i.e. free Atto 655 biotin.

References

1. B. Derby, *Annual Review of Materials Research*, 2010, **40**, 395–414.
2. H. Dong, W. W. Carr, and J. F. Morris, *Physics of Fluids*, 2006, **18**, 072102.
3. J. Eggers, *Reviews of Modern Physics*, 1997, **69**, 865–930.
4. B. K. L. and Y. C. L. H.Y. Gan, X. Shan, T. Eriksson, *Journal of Micromechanics and Microengineering*, 2009, **19**, 55010.
5. O. Krichevsky and G. Bonnet, *Reports on Progress in Physics*, 2002, **65**, 251.
6. A. Illaste, M. Laasmaa, P. Peterson, and M. Vendelin, *Biophysical Journal*, 2012, **102**, 739–748.